AIAA JOURNAL
Vol. 42, No. 1, January 2004

Modified k–ε Turbulence Model for Calculating Hot Jet Mean Flows and Noise

Christopher K. W. Tam* and Anand Ganesan†
Florida State University, Tallahassee, Florida 32306-4510

The k–ε model has no provision to include the effect of the presence of a large-density gradient when used to compute the mean flow and noise of very hot jets. As a result, the model is found to give good predictions only when the jet is cold or moderately hot. Stability consideration indicates that a large density difference across a shear layer would generate strong spatial Kelvin–Helmholtz instabilities. Such instabilities would, invariably, lead to intense mixing in the jet shear layer. This, in turn, gives rise to an increase in turbulence intensity and jet spreading rate. A modification to the k–ε model is proposed to mimic these effects. Computed mean flow profiles and centerline velocity distributions of high-temperature jets using the modified k–ε model are found to compare well with experimental measurements. The accuracy of noise predictions for hot jets is also found to improve when the density gradient is taken into account.

Nomenclature

$c_\mu, c_{\varepsilon 1}, c_{\varepsilon 2}, c_{\varepsilon 3}, \sigma_T, \sigma_k, \sigma_\varepsilon, \alpha_1$	=	parameters of k–ε model and modifications
D	=	nozzle exit diameter
k	=	turbulence kinetic energy per unit mass
M_j	=	jet Mach number
Pr	=	turbulent Prandtl number
T_j	=	jet exit temperature
u_j	=	jet exit velocity
δ_{ij}	=	Kronecker delta
ε	=	dissipation rate of the k–ε model
ν_t	=	turbulent eddy viscosity
ρ_j	=	jet exit density
τ_{ij}	=	turbulent stresses

I. Introduction

THE k–ε turbulence model has been widely used in association with the Reynolds averaged Navier–Stokes equations (RANS) for calculating various types of turbulent mean flows for engineering applications. However, note that the applicability of the original k–ε model is quite limited. This is because the model contains only a bare minimum of turbulence physics. Also it is because the unknown constants of the original model[1–4] were calibrated primarily by using low-Mach-number boundary layer and two-dimensional mixing layer flow data.

The useful range of the k–ε model has since been extended. The extensions were carried out in two ways. First, a number of correction terms, intended to incorporate additional turbulence physics to the model, were proposed. Notable model corrections are the Pope correction[5] developed for use in three-dimensional jets and the Sarkar and Lakshmanan correction[6] developed for use when the flow convective Mach number is not too small. Second, for application to a specific class of turbulent flows, the empirical constants of the original model were recalibrated using a larger set of more appropriate data. The motivation for recalibration is the recognition that these constants are not really universal. The model would have a much better chance to be successful if it is applied to a restricted class of flows with similar turbulent mixing characteristics. For each class of flows, a new but more suitable set of constants is used. For instance, for calculating axisymmetric and three-dimensional jet mean flows, Thies and Tam[7] recalibrated the unknown model constants by using a large set of jet flow data covering a wide range of Mach numbers. Their computed jet mean flow velocity profiles for ambient temperature jets were found to be in excellent agreement with experimental measurements. More recently, applications of the recalibrated model to jets in simulated forward flight, coaxial jets, and jets with inverted velocity profile[8] have been carried out. (Data of these types of flows were not included in the recalibration.) The calculated velocity profiles were again found to be in good agreement with experiments.

Recently, Tam and Auriault[9] developed a theory by which the noise spectrum from the fine-scale turbulence of a jet can be calculated. This theory takes into account the mean flow refraction effect, as well as the effect of noise source motion. The turbulence information required by the theory such as the turbulence intensity and its length and time decay scales are supplied by the k–ε turbulence model as modified by Thies and Tam.[7] For cold and moderately hot jets, the computed noise spectra compare well with measured data over a wide range of jet Mach numbers and directions of radiation.

For hot jets, both the mean flow and noise predictions based on the recalibrated k–ε turbulence model are found not to be as good. In this paper, it will be shown that hot jets spread faster than that given by the model theory. Also, the noise level and the peak frequency of the calculated spectrum are slightly off. An examination of the k–ε turbulence model indicates that the model has no provision for jet temperature or density effect. Experimentally, it is known[10,11] that the spreading rate of a two-dimensional shear layer or the mixing layer of a jet is affected by the density difference across the layer.

The objective of this work is to examine the flow physics of hot jets especially the dependence of its mixing characteristics on gas densities. It is determined that the density difference between the ambient gas and that of a hot jet would promote strong flow instabilities, which, in turn, lead to faster mixing and spreading of the jet flow. Based on this observation, a modified k–ε model is proposed. The modification is designed specifically to result in enhanced mixing whenever a strong density gradient (in opposite direction to that of the mean flow) is present in the jet flow. Calculated jet mean velocity profiles at elevated jet temperature based on the modified k–ε model are provided in the paper. It will be shown that the calculated profiles are in good agreement with measured data over a wide range of jet Mach numbers and temperature ratios. Furthermore, by using the turbulence information provided by the modified k–ε model, the noise spectra as calculated by the Tam and Auriault theory[9] are

Received 16 September 2002; revision received 23 June 2003; presented as Paper 2002-1064 at the 41st Aerospace Sciences Meeting, Reno, NV, 6–9 January 2003; accepted for publication 14 July 2003.

*Robert O. Lawton Distinguished Professor, Department of Mathematics; tam@math.fsu.edu. Fellow AIAA.
†Graduate Student, Department of Mathematics.

found to agree well with measurements. The modification on the k–ε model significantly improves the accuracy of its prediction.

Since the appearance of a preliminary version of this paper,[12] there have been other attempts to modify the k–ε model to include temperature or density effect. Recently Massey et al.[13] proposed a simple modification to the model intended for wall-bounded turbulent flow applications. However, the model lacks generality. The authors recommended its use to be restricted to subsonic flows. Birch et al.[14] considered the use of the k–ε model for hot coaxial jets issued from chevron nozzles. They proposed a zonal model in which different corrections were implemented in different regions of the dual-flow stream. Understandably, such a model necessarily contains more empiricism. It is also not applicable to more general turbulent shear flows.

II. Jet Flow k–ε Model

Dimensionless variables with D, u_j, ρ_j, T_j, nozzle exit diameter, velocity, density, and temperature as the length, velocity, density, and temperature scales will be used. Time, pressure, and the turbulence quantities k and ε will be nondimensionalized by D/u_j, $\rho_j u_j^2$, u_j^2, and u_j^3/D, respectively. Turbulent stresses τ_{ij} and eddy viscosity ν_t will be nondimensionalized by u_j^2 and $u_j D$. In Cartesian tensor notation, the Favre-averaged equations of motion including the k–ε model as well as the Pope[5] and Sarkar and Lakshmanan[6] correction terms in dimensionless form are

$$\frac{\partial u_\ell}{\partial x_\ell} = \frac{u_\ell}{T}\frac{\partial T}{\partial x_\ell} - \frac{u_\ell}{p}\frac{\partial p}{\partial x_\ell} \tag{1}$$

$$\rho u_\ell \frac{\partial u_i}{\partial x_\ell} = -\frac{\partial p}{\partial x_i} - \frac{\partial(\rho\tau_{i\ell})}{\partial x_\ell} \tag{2}$$

$$\rho u_\ell \frac{\partial T}{\partial x_\ell} = -\gamma(\gamma-1)M_j^2 p\frac{\partial u_\ell}{\partial x_\ell} + \gamma(\gamma-1)M_j^2\rho\varepsilon + \frac{\gamma}{P_r}\frac{\partial}{\partial x_\ell}\left(\rho\nu_t\frac{\partial T}{\partial x_\ell}\right) \tag{3}$$

$$\rho u_\ell \frac{\partial k}{\partial x_\ell} = -\rho\tau_{i\ell}\frac{\partial u_i}{\partial x_\ell} - \rho\varepsilon + \frac{1}{\sigma_k}\frac{\partial}{\partial x_\ell}\left(\rho\nu_t\frac{\partial k}{\partial x_\ell}\right) \tag{4}$$

$$\rho u_\ell \frac{\partial \varepsilon_s}{\partial x_\ell} = -C_{\varepsilon 1}\frac{\varepsilon_s}{k}\rho\tau_{i\ell}^s\frac{\partial u_i}{\partial x_\ell} - (C_{\varepsilon 2} - C_{\varepsilon 3}\chi)\rho\frac{\varepsilon_s^2}{k} + \frac{1}{\sigma_\varepsilon}\frac{\partial}{\partial x_\ell}\left(\rho\nu_t^s\frac{\partial \varepsilon_s}{\partial x_\ell}\right) \tag{5}$$

$$p = \frac{1}{\gamma M_j^2}\rho T \tag{6}$$

$$\nu_t = c_\mu\frac{k^2}{\varepsilon}, \qquad \nu_t^s = c_\mu\frac{k^2}{\varepsilon_s} \tag{7}$$

$$\varepsilon = \varepsilon_s\left(1 + \alpha_1 M_t^2\right) \tag{8}$$

$$M_t^2 = \frac{2k}{T}M_j^2 \tag{9}$$

$$\tau_{i\ell} = \frac{2}{3}k\delta_{i\ell} - \nu_t\left(\frac{\partial u_i}{\partial x_\ell} + \frac{\partial u_\ell}{\partial x_i} - \frac{2}{3}\frac{\partial u_j}{\partial x_j}\delta_{i\ell}\right) \tag{10}$$

$$\tau_{i\ell}^s = \frac{2}{3}k\delta_{i\ell} - \nu_t^s\left(\frac{\partial u_i}{\partial x_\ell} + \frac{\partial u_\ell}{\partial x_i} - \frac{2}{3}\frac{\partial u_j}{\partial x_j}\delta_{i\ell}\right) \tag{11}$$

$$\chi = \omega_{ij}\omega_{j\ell}S_{\ell i} \tag{12}$$

$$\omega_{ij} = \frac{1}{2}\frac{k}{\varepsilon_s}\left(\frac{\partial u_i}{\partial x_j} - \frac{\partial u_j}{\partial x_i}\right) \tag{13}$$

$$s_{i\ell} = \frac{1}{2}\frac{k}{\varepsilon_s}\left(\frac{\partial u_i}{\partial x_\ell} + \frac{\partial u_\ell}{\partial x_i}\right) \tag{14}$$

where γ is the ratio of specific heats.

Equation (1) is derived from the continuity equation with ρ eliminated in favor of p and T by the equation of state. There are eight empirical constants in the preceding system. Here, the values recommended by Thies and Tam[7] are adopted:

$$c_\mu = 0.0874, \qquad c_{\varepsilon 1} = 1.40, \qquad c_{\varepsilon 2} = 2.02, \qquad c_{\varepsilon 3} = 0.822$$
$$\gamma\sigma_T = Pr = 0.422, \qquad \sigma_k = 0.324$$
$$\sigma_\varepsilon = 0.377, \qquad \alpha_1 = 0.518 \tag{15}$$

By using these constants, Thies and Tam demonstrated that the k–ε model can yield good predictions of jet mean flow profiles for cold and moderately hot axisymmetric jets over the Mach number range of 0.4–2.22. They also showed that the model gives reasonable mean velocity prediction for cold elliptic and rectangular jets in the Mach number range of 0.4–1.5. Recently, Tam et al.[8] applied the k–ε model with the preceding constants for the prediction of cold jets in simulated forward flight, the mean flows of coaxial jets, and jets with inverted velocity profile. The predictions were in good agreement with experimental measurements.

In this paper, the preceding system of equations is solved by first putting it in a parabolized form. The steps involved in parabolization are as follows: 1) The $\partial p/\partial x$ term in the x-momentum equation is dropped (boundary-layer approximation) where the x axis coincides with the centerline axis of the jet. 2) All eddy viscosity terms involving x derivatives are neglected. They are small compared with derivatives in the transverse or radial direction. 3) All of the diffusion terms involving x derivatives are neglected. They are small compared with diffusion in the transverse direction. 4) Outside the jet, it is assumed that there is a uniform mean flow equal to 2% or less of the jet exit velocity. This is strictly a parabolization approximation. This approximation allows one to march the solution downstream. If $\boldsymbol{u}$ is the flow vector consisting of all of the flow variables, that is,

$$\boldsymbol{u} = (p, u, v, w, T, k, \varepsilon)^T \tag{16}$$

where superscript T denotes the transpose, then the fully parabolized equation may be written in the form

$$\frac{\partial \boldsymbol{u}}{\partial x} = \boldsymbol{F} \tag{17}$$

For axisymmetric jets, $\boldsymbol{F}$ is given in full in Appendix A.

The fully parabolized equation (17) is slightly different from that actually used in the computation of Thies and Tam.[7] Thies and Tam employed the boundary-layer approximation $p = \text{const}$. This is not used here. Also in their work, the radial velocity component v is calculated by solving the continuity equation implicitly after each forward marching step has been completed. In the present work, the full set of variables is solved by marching in the downstream direction using the dispersion-relation-preserving scheme.[15] Details of the grid design and artificial selective damping used are discussed in Appendix B.

Figure 1a shows the computed profiles of the axial velocity component of a Mach 0.8 jet at temperature ratio $T_r/T_a = 1.686$, where T_r and T_a are the reservoir and ambient temperature, respectively. Figure 1a also shows the experimental measurements of Lepicovsky et al.[16] Figure 1b shows a comparison of the computed and measured centerline velocity. As can be seen, at moderately high temperature, the calculated velocity profiles and centerline velocity distribution based on the k–ε model and the coefficients of Thies and Tam[7] are in good agreement with measurements. However, for higher temperature jets, there is an increasing deviation between predictions and measurements. Figure 2a shows the case of a Mach 0.8 jet at temperature ratio 2.317. Figure 2b shows the corresponding comparison of the jet centerline velocity distribution. Figures 2a and 2b clearly indicate that starting at $x/D = 5.0$ (where D is the jet diameter) the model overpredicts the centerline velocity. This

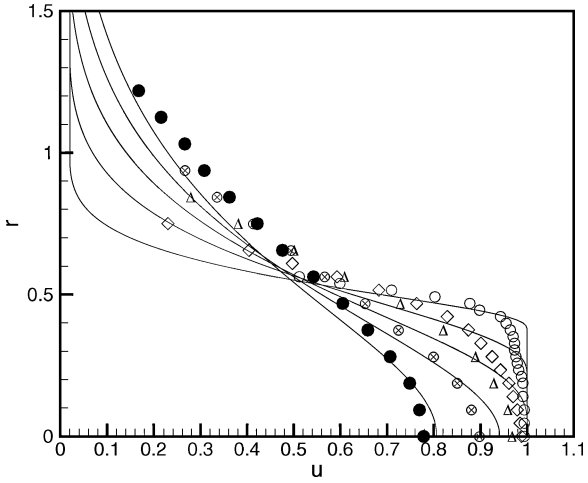

Fig. 1a Comparisons between computed and measured axial velocity profiles; data from Lepicovsky et al.,[16] Mach 0.8, $T_r/T_a = 1.69$ jet: ○, $x = 1.0$; ◇, $x = 3.0$; Δ, $x = 5.0$; ⊗, $x = 7.0$; ●, $x = 9.0$; and ——, k–ϵ model.

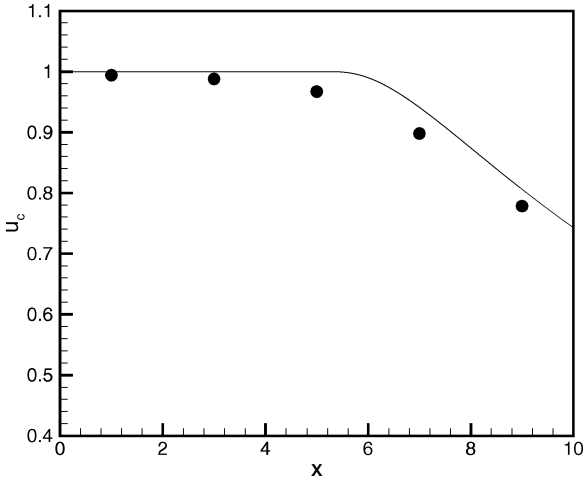

Fig. 1b Comparison between computed jet centerline velocity and the measurements of Lepicovsky et al.,[16] Mach 0.8, $T_r/T_a = 1.69$: ●, measurement and ——, k–ϵ model.

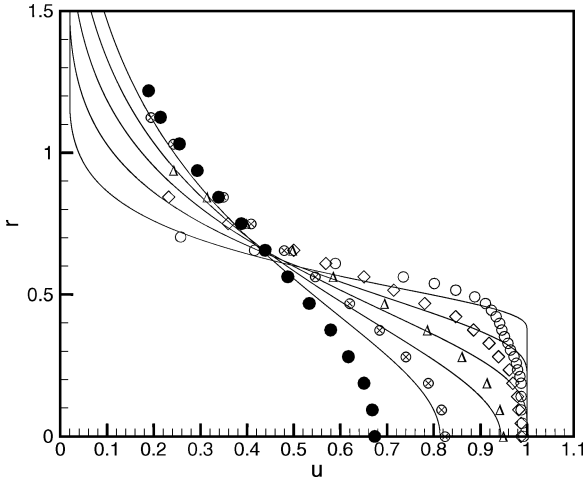

Fig. 2a Comparisons between computed and measured axial velocity profiles; data from Lepicovsky et al.,[16] Mach 0.8, $T_r/T_a = 2.32$ jet: ○, $x = 1.0$; ◇, $x = 3.0$; Δ, $x = 5.0$; ⊗, $x = 7.0$; ●, $x = 9.0$; and ——, k–ϵ model.

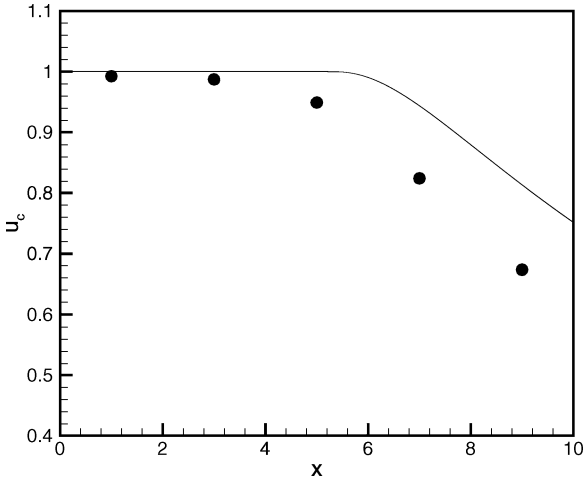

Fig. 2b Comparison between computed jet centerline velocity and the measurements of Lepicovsky et al.,[16] Mach 0.8, $T_r/T_a = 2.32$: ●, measurement, and ——, k–ϵ model.

overprediction increases in the downstream direction. Other examples (shown later) reinforce this observation. Because the Sarkar and Lakshmanan correction,[6] which mimics the effect of convective Mach number, is included in the calculation, it is believed that the discrepancy is the result of the large density difference between the jet and ambient gas. As stated before, experimental observations indicate that a strong density gradient across a mixing layer could have an important influence on its rate of spread.[10,11] The k–ε model has no provision for density gradient. It would appear, therefore, that a modification of the k–ε model to include the density effect is necessary if the model is to be successful in calculating the mean velocity profiles of hot jets.

III. Physics of Hot Jets

It is now known that the fluid dynamics in the mixing layer of a jet is largely controlled by the large turbulence structures of the flow. These large structures are intrinsically related to the instabilities of the mixing layer. To investigate the effect of density on the dynamics of turbulent mixing, it is useful to see how the density difference across the mixing layer affects the instabilities of the layer. To keep the analysis simple, we will consider the Kelvin–Helmholtz instability of two incompressible fluid layers of density ρ_1 and ρ_2 separated by a vortex sheet moving relative to each other at a velocity U as shown in Fig. 3. Let subscripts 1 and 2 be used to denote the variables in layers 1 and 2 and $y = \zeta(x, t)$ be the displacement of the vortex sheet where x is in the direction of flow

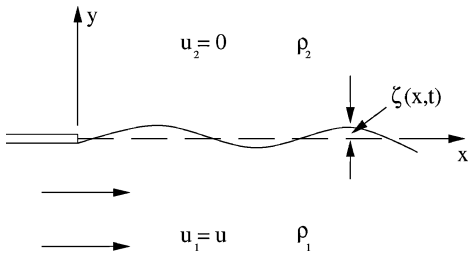

Fig. 3 Kelvin–Helmholtz instability at the interface of two fluid layers of different densities.

and y is normal to the fluid layers. Mathematically, the instability problem is

$$\nabla \cdot \boldsymbol{v}_1 = 0, \qquad \rho_1 \left(\frac{\partial \boldsymbol{v}_1}{\partial t} + U \frac{\partial \boldsymbol{v}_1}{\partial x} \right) = -\nabla p_1 \tag{18}$$

$$\nabla \cdot \boldsymbol{v}_2 = 0, \qquad \rho_2 \frac{\partial \boldsymbol{v}_2}{\partial t} = -\nabla p_2 \tag{19}$$

The kinematic boundary conditions at $y = 0$ are

$$\frac{\partial \zeta}{\partial t} + U \frac{\partial \zeta}{\partial x} = v_1, \qquad \frac{\partial \zeta}{\partial t} = v_2 \tag{20}$$

The dynamic boundary condition at $y=0$ is

$$p_1 = p_2 \tag{21}$$

The solution of the preceding instability problem is known, for example, by Landau and Lifshitz.[17] It is conceivable that the problem has also been solved by others. For instability wave solution of the form

$$p_1(x, y, t) = \hat{p}_1(y)e^{i(\alpha x - \omega t)} \tag{22}$$

and similar dependence for all other variables, it is easy to show that the dispersion relation that links frequency ω to wave number α is given by

$$(\omega - \alpha U)^2 = -(\rho_2/\rho_1)\omega^2 \tag{23}$$

Our interest is in spatial instability. Thus, on solving for α, we find

$$\alpha = \omega/U \pm i(\rho_2/\rho_1)^{\frac{1}{2}}(\omega/U) \tag{24}$$

The root with negative imaginary part is the unstable root. The spatial growth rate is given by the imaginary part of α, that is,

$$\mathrm{Im}(\alpha) = (\rho_2/\rho_1)^{\frac{1}{2}}(\omega/U) \tag{25}$$

Equation (25) suggests that the growth rate is affected by the density ratio ρ_2/ρ_1. For hot jets $\rho_1 < \rho_2$; hence, there is an increase in growth rate due to density difference. This means that there will be stronger mixing and larger shear layer spreading rate for very hot jets. Therefore, the density effect should be incorporated in the k–ε model for hot-jet mean flow calculations.

IV. Modified k–ε Model

The k–ε model is a very simple turbulence model. The turbulence at a point is characterized by two quantities, k and ε. Within the framework of the model, turbulent mixing and, hence, the spreading rate of a mixing layer are controlled by the turbulent viscosity $\nu_t = c_\mu k^2/\varepsilon$. Thus, a simple way to incorporate the density effect on turbulent mixing is to allow ν_t to depend on density gradient.

Let us first consider the special case of axisymmetric jets. The density effect is then characterized locally by $(1/\rho)(\partial\rho/\partial r)$. The k–ε model is a local model, so that any modification should be on a local basis. We will assume that the effect of density on turbulent mixing is relatively small. As a first approximation, it is reasonable to take the density effect to be a linear addition to the original eddy viscosity. We expect the linear term added to be small so that it may be regarded as a perturbation on the original turbulent mixing. In other words, let ν_T be the combined eddy viscosity (including density effect on flow instabilities). We will assume

$$\nu_T = \nu_t + \nu_\rho \tag{26}$$

where ν_ρ is the density effect and $\nu_t = c_\mu k^2/\varepsilon$ is the original turbulent eddy viscosity. It will further be assumed that ν_ρ is linearly dependent on $(1/\rho)(\partial\rho/\partial r)$. Now ν_ρ must have the dimensions of kinematic viscosity. To ensure dimensional balance in Eq. (26), note that, within the k–ε model, there are only two other quantities, that is, k and ε, available for dimensional adjustment. A simple dimensional analysis yields the following relation:

$$\nu_\rho = \begin{cases} c_\rho \dfrac{k^{\frac{7}{2}}}{\varepsilon^2}\dfrac{1}{\rho}\left|\dfrac{\partial\rho}{\partial r}\right|, & \text{if } \dfrac{\partial\rho}{\partial r} \text{ is opposite in sign to } \dfrac{\partial u}{\partial r} \\ 0, & \text{otherwise} \end{cases} \tag{27}$$

The unknown constant c_ρ is assigned the numerical value 0.035 by best fit to the data.

In Eq. (27), ν_ρ is set equal to zero unless the jet is hot. (No modification is needed.) This is suggested by the result of the instability analysis of Sec. III. There, it was found that only when the less dense fluid moved faster would it result in an increase in the Kelvin–Helmholtz instability wave growth rate. This, in turn, would lead to an increase in turbulent mixing. In the proposed modification, an increase in turbulent mixing is achieved by an increase in the turbulent eddy viscosity of the k–ε model.

For applications to nonaxisymmetric jets or for jets issued from internal mixer nozzles, formula (27) may be generalized as follows. It will be assumed that these jets diverge slowly in the axial direction. Again, let x be in the jet flow direction. Then u and ρ are slowly varying functions of x. The reference direction for the shearing flow motion is ∇u. The relevant part of the density gradient that affects mixing is the projection of $\nabla\rho$ on ∇u. A simple generalization of the contribution of density effect on turbulent eddy viscosity is

$$\nu_\rho = \begin{cases} c_\rho \dfrac{k^{\frac{7}{2}}}{\varepsilon^2}\dfrac{1}{\rho}\dfrac{|(\nabla\rho)\cdot(\nabla u)|}{|\nabla u|}, & \text{if } (\nabla u)\cdot(\nabla\rho) \text{ is negative} \\ 0, & \text{otherwise} \end{cases}$$

V. Numerical Results

We will now demonstrate that if the present proposed modification to the k–ε model is adopted, the agreement between computed and experimentally measured mean flow profiles and centerline velocity distributions are substantially improved, even when the jet temperature is very high. For this purpose, note that hot-jet flow data are difficult to measure. As a result, only a limited set of data is available in the open literature.

Figures 4a and 4b show comparisons between computed and measured axial velocity profiles of a Mach 0.8 jet at a temperature ratio of 2.32. The data are from Lepicovsky et al.[16] Both the computed profiles with and without density correction are shown. Figure 4c shows a comparison of the corresponding centerline velocity. Similar comparisons for a Mach 0.8 jet at a higher temperature ratio of 2.79, a Mach 1.0 jet at temperature ratio of 2.32 and a Mach 0.48 jet at temperature ratio of 1.69 are given in Figs. 5–7. It is evident from these comparisons that the inclusion of density correction greatly improves the accuracy of the k–ε model predictions at elevated jet temperature. This is true for jets at low subsonic Mach number as well as at sonic Mach number.

We will now demonstrate that the proposed density correction also works well for supersonic jets. Figure 8a shows comparisons of computed and measured centerline velocity and half velocity point distributions of a Mach 2.0 jet at temperature ratio 2.72. The measurements are from Seiner et al.[18] The computed centerline velocity distributions for cases with and without density correction are provided. Figure 9 shows similar comparisons for a Mach 2.0 jet at a much higher temperature ratio of 4.0. When the computed results are compared with experimental measurements shown in Figs. 8 and 9, it is readily seen that the inclusion of the proposed density correction improves the predicted results for hot supersonic jets. This is especially true for centerline velocity beyond the potential core.

The proposed density correction, no doubt, will have an effect on the predicted distribution of turbulence intensity. However, quality data of k for hot jets are presently not available to allow an assessment of the accuracy of the model.

Recently, Tam and Auriault[9] developed a theory for predicting the fine-scale turbulence noise of high-speed jets. The fine-scale turbulence noise is the dominant noise component in the sideline direction. This theory is closely tied to the k–ε model. The turbulence information needed for noise prediction such as turbulence intensity, the turbulence decay time, and the size of fine-scale turbulence are supplied by the k–ε model. The Tam and Auriault theory also takes mean flow refraction into consideration. This is accounted for by the use of an adjoint Green's function. The mean flow refraction effect and the adjoint Green's function depend on the mean flow profile. In the work of Tam and Auriault, the mean profiles of the jets are calculated by the k–ε model.

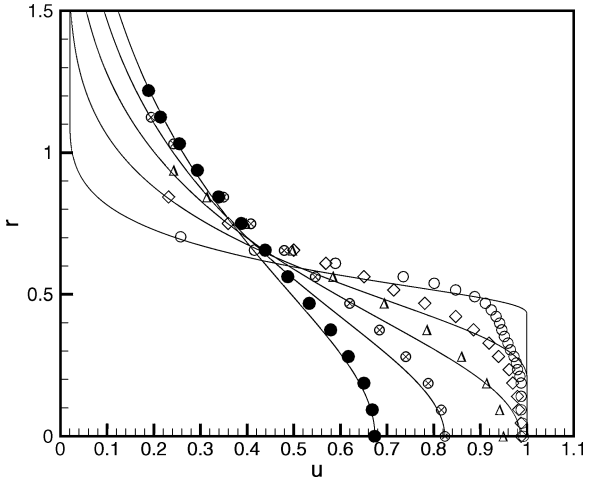

Fig. 4a Comparisons between computed and measured axial velocity profiles; data from Lepicovsky et al.,[16] Mach 0.8, $T_r/T_a = 2.32$ jet: ○, $x = 1.0$; ◇, $x = 3.0$; Δ, $x = 5.0$; ⊗, $x = 7.0$; ●, $x = 9.0$; and ——, with density correction.

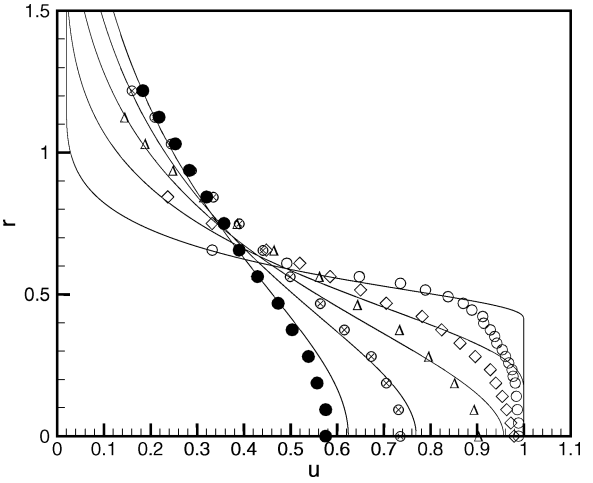

Fig. 5a Comparisons between computed and measured axial velocity profiles; data from Lepicovsky et al.,[16] Mach 0.8, $T_r/T_a = 2.79$ jet: ○, $x = 1.0$; ◇, $x = 3.0$; Δ, $x = 5.0$; ⊗, $x = 7.0$; ●, $x = 9.0$; and ——, with density correction.

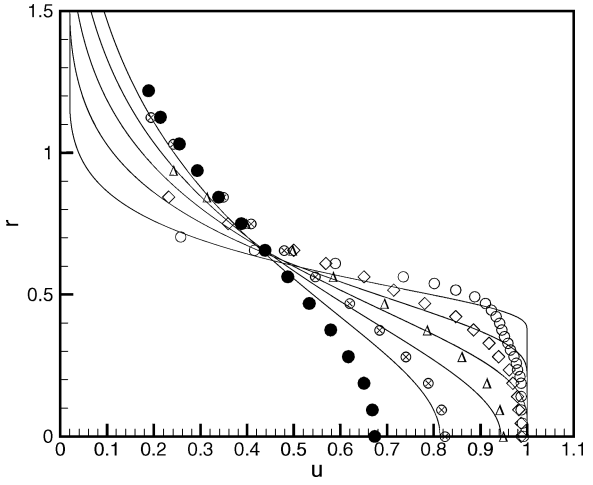

Fig. 4b Comparisons between computed and measured axial velocity profiles; data from Lepicovsky et al.,[16] Mach 0.8, $T_r/T_a = 2.32$ jet: ○, $x = 1.0$; ◇, $x = 3.0$; Δ, $x = 5.0$; ⊗, $x = 7.0$; ●, $x = 9.0$; and ——, without density correction.

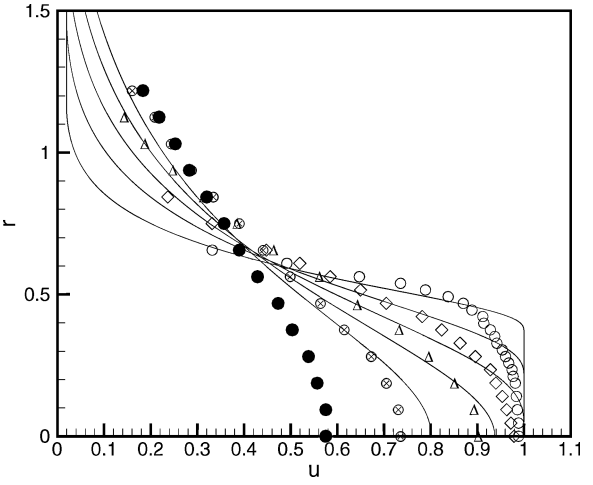

Fig. 5b Comparisons between computed and measured axial velocity profiles; data from Lepicovsky et al.,[16] Mach 0.8, $T_r/T_a = 2.79$ jet: ○, $x = 1.0$; ◇, $x = 3.0$; Δ, $x = 5.0$; ⊗, $x = 7.0$; ●, $x = 9.0$; and ——, without density correction.

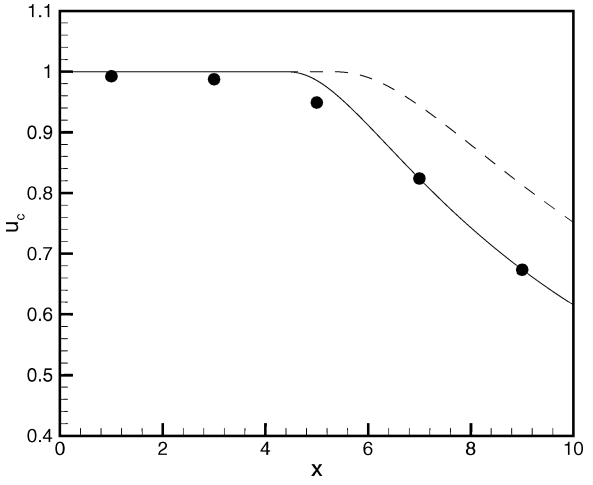

Fig. 4c Comparison between computed jet centerline velocity and the measurements of Lepicovsky et al.,[16] Mach number 0.8, $T_r/T_a = 2.32$: ●, measurement; ——, with density correction; and – – –, without density correction.

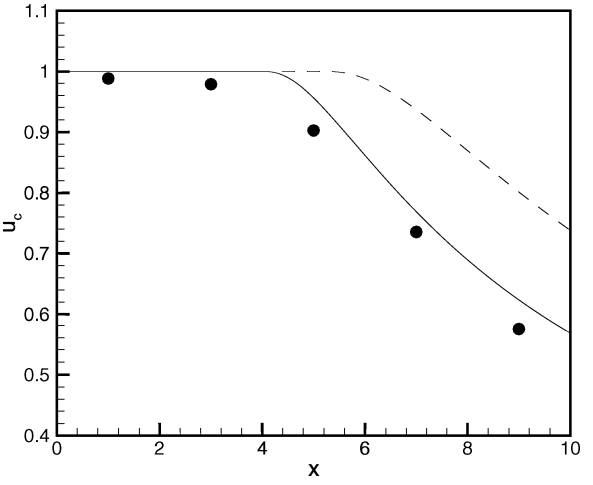

Fig. 5c Comparison between computed jet centerline velocity and the measurements of Lepicovsky et al.,[16] Mach number 0.8, $T_r/T_a = 2.79$: ●, measurement; ——, with density correction; and – – –, without density correction.

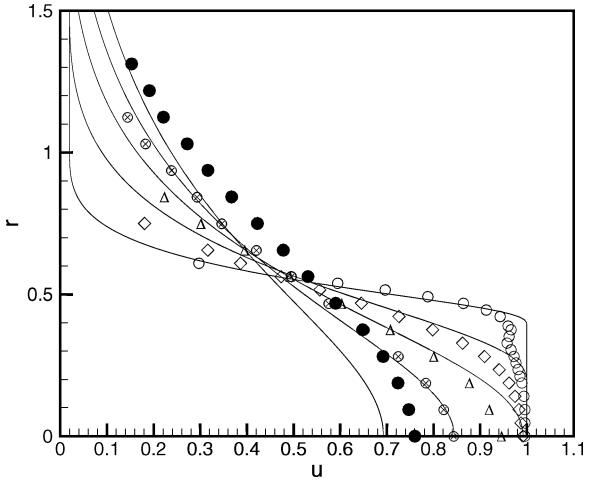

Fig. 6a Comparisons between computed and measured axial velocity profiles; data from Lepicovsky et al.,[16] Mach 1.0, $T_r/T_a = 2.32$ jet: ○, $x = 1.0$; ◇, $x = 3.0$; Δ, $x = 5.0$; ⊗, $x = 7.0$; ●, $x = 9.0$; and ——, with density correction.

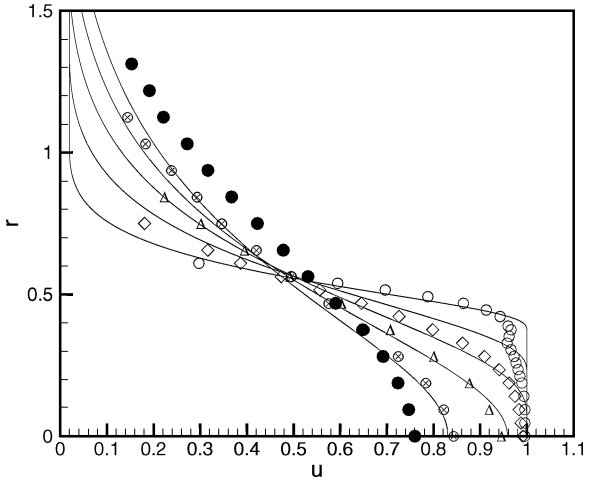

Fig. 6b Comparisons between computed and measured axial velocity profiles; data from Lepicovsky et al.,[16] Mach 1.0, $T_r/T_a = 2.32$ jet: ○, $x = 1.0$; ◇, $x = 3.0$; Δ, $x = 5.0$; ⊗, $x = 7.0$; ●, $x = 9.0$; and ——, without density correction.

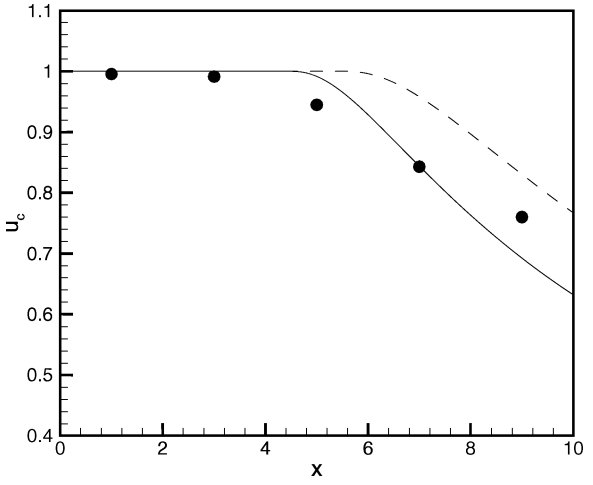

Fig. 6c Comparison between computed jet centerline velocity and the measurements of Lepicovsky et al.,[16] Mach number = 1.0, $T_r/T_a = 2.32$: ●, measurement; ——, with density correction; and – – –, without density correction.

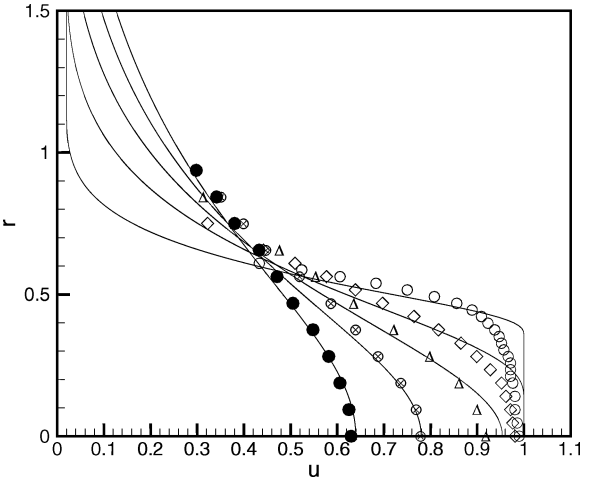

Fig. 7a Comparisons between computed and measured axial velocity profiles; data from Lepicovsky et al.,[16] Mach 0.48, $T_r/T_a = 1.69$ jet: ○, $x = 1.0$; ◇, $x = 3.0$; Δ, $x = 5.0$; ⊗, $x = 7.0$; ●, $x = 9.0$; and ——, with density correction.

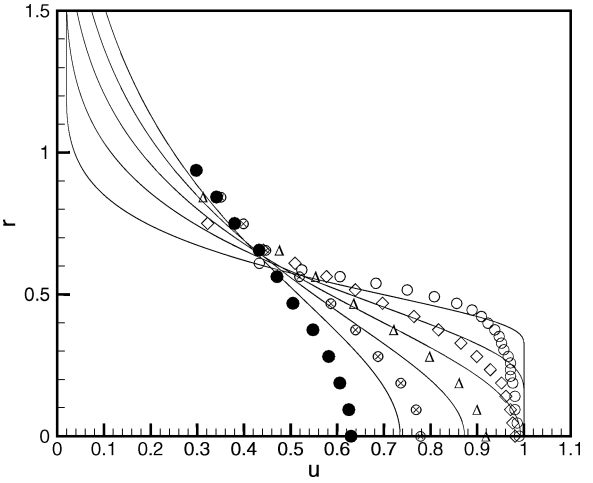

Fig. 7b Comparisons between computed and measured axial velocity profiles; data from Lepicovsky et al.,[16] Mach 0.48, $T_r/T_a = 1.69$ jet: ○, $x = 1.0$; ◇, $x = 3.0$; Δ, $x = 5.0$; ⊗, $x = 7.0$; ●, $x = 9.0$; and ——, without density correction.

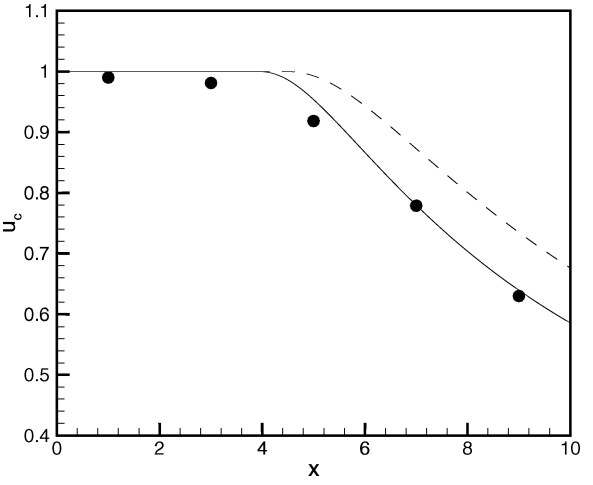

Fig. 7c Comparison between computed jet centerline velocity and the measurements of Lepicovsky et al.,[16] Mach number 0.48, $T_r/T_a = 1.69$: ●, measurement; ——, with density correction; and – – –, without density correction.

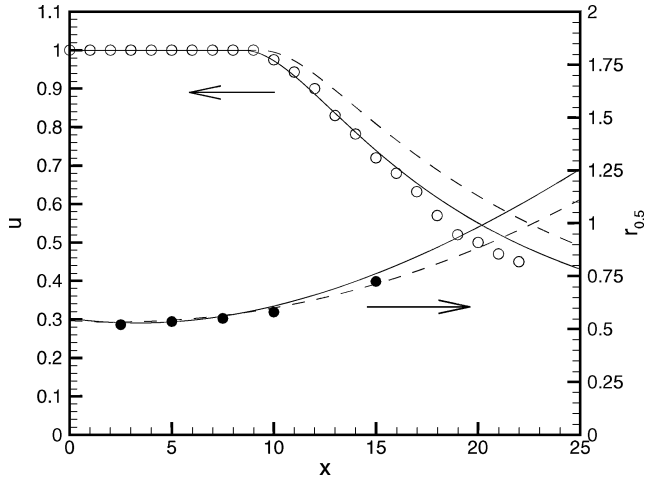

Fig. 8 Comparisons between computed jet centerline velocity and half-velocity point distributions and the measurements of Seiner et al.,[18] Mach number 2.0, $T_r/T_a = 2.718$: ○, measured centerline velocity; ●, measured half-velocity point; ——, with density correction; and – – –, without density correction.

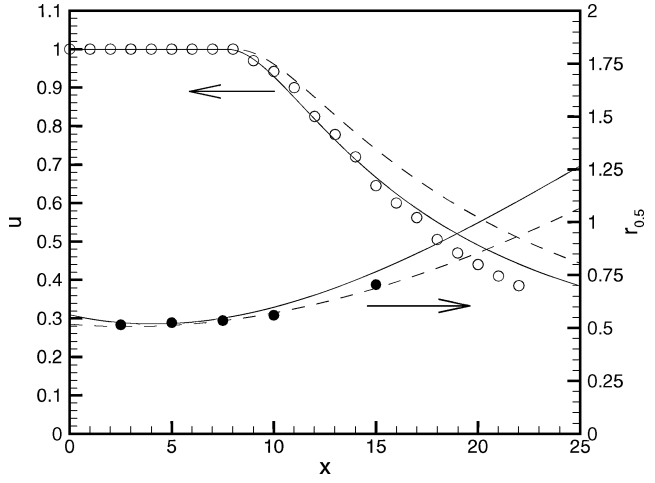

Fig. 9 Comparisons between computed jet centerline velocity and half-velocity point distributions and the measurements of Seiner et al.,[18] Mach number 2.0, $T_r/T_a = 4.0$: ○, measured centerline velocity; ●, measured half-velocity point; ——, with density correction; and – – –, without density correction.

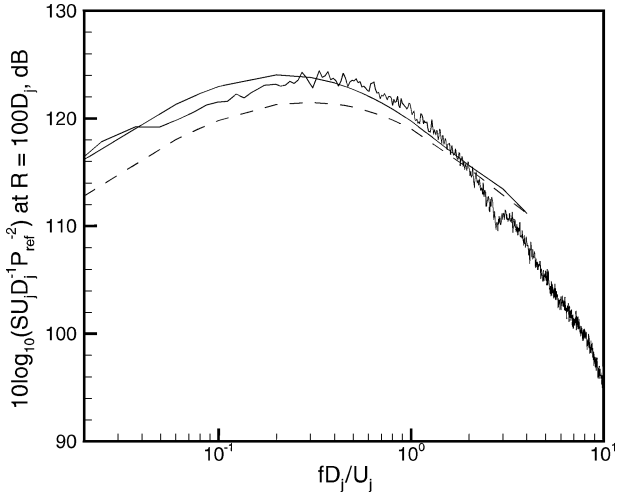

Fig. 10 Noise spectrum at 88.6 deg (inlet angle) from a Mach 2.0 jet at temperature ratio 3.28; data from Seiner et al.,[18] and theory from Tam and Auriault[9]: ——, with density correction and – – –, without density correction.

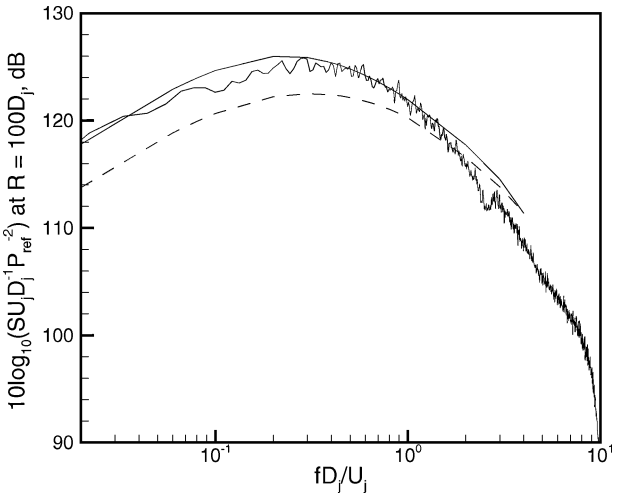

Fig. 11 Noise spectrum at 88.6 deg (inlet angle) from a Mach 2.0 jet at temperature ratio 4.07; data from Seiner et al.,[18] and theory from Tam and Auriault[9]: ——, with density correction and – – –, without density correction.

The Tam and Auriault theory[9] has proven to be the most successful jet noise theory up to the present time. For cold and moderately hot jets the predictions of the theory are in good agreement with experiments. The theory has since been applied to jets in simulated forward flight[8] and to nonaxisymmetric jets[19] with equal success. These later applications are again restricted to cold and moderately hot jets.

The present proposed density correction to the k–ε model, invariably, will have an impact on the ability of the Tam and Auriault theory[9] in predicting hot-jet noise spectra. Figure 10 shows comparisons between computed noise spectra of a Mach 2.0 jet at 88.6 deg measured from nozzle inlet and the experimental measurements of Seiner et al.[18] The temperature ratio of the jet is 3.28. It is clear that the calculated spectrum with density correction is in better agreement with experiment. Figure 11 shows a similar comparison for an even higher temperature ratio of 4.07. Again, the inclusion of density correction improves the accuracy of the prediction.

VI. Conclusions

A modification to the k–ε model aimed to extend its applicability to the computation of the mean flow and noise of high-speed hot jets is proposed. The motivation of the proposal arises from the observation that there is a large density-induced increase in the growth rate of spatial instabilities of a mixing layer if the lighter fluid moves faster. This consideration leads to the incorporation of a density gradient related contribution to the turbulent eddy viscosity of the k–ε model. Computed jet mean flow profiles and centerline velocity distributions at elevated temperatures of high-speed jets are found to be in better agreement with experimental measurements if density modification is included. Noise predictions including the density effect are also found to be in better agreement with microphone measurements. The good agreements offer strong support to the validity and usefulness of the proposed density correction formula.

Note that the density correction proposed here is strictly intended for use in jets and free shear flows. Whether the use of the same correction would lead to similar good predictions for wall-bounded turbulent flows is beyond the scope of the present work. This should not be difficult to understand. The reason is that the role of large turbulence structures in free shear flows is not the same as in wall-bounded flows. We would, therefore, like to suggest that care should be exercised when considering the application of the proposed correction to turbulent flows in which the turbulent mixing dynamics and large flow structures are substantially different from those of turbulent free shear layers.

Appendix A: Fully Parabolized Equations for Axisymmetric Jets

For axisymmetric jets, the parabolized RANS equations with k–ε model [Eq. (17)] in cylindrical coordinates are

$$\frac{\partial u}{\partial x}=\frac{1}{\rho u}\left[-\rho v\frac{\partial u}{\partial r}-\frac{1}{r}\frac{\partial}{\partial r}(\rho\tau_{rx}r)\right]$$

$$\frac{\partial v}{\partial x}=\frac{1}{\rho u}\left[-\rho v\frac{\partial v}{\partial r}-\frac{\partial p}{\partial r}-\frac{1}{r}\frac{\partial}{\partial r}(\rho\tau_{rr}r)+\frac{\rho\tau_{\phi\phi}}{r}\right]$$

$$\frac{\partial T}{\partial x}=\frac{1}{\rho u}\left[-\rho v\frac{\partial T}{\partial r}-\gamma(\gamma-1)M_j^2 p\left(\frac{\partial v}{\partial r}+\frac{v}{r}+\frac{\partial u}{\partial x}\right)\right.$$
$$\left.+\gamma(\gamma-1)M_j^2\rho\varepsilon+\frac{\gamma}{p_r}\frac{1}{r}\frac{\partial}{\partial r}\left(\rho\nu_t r\frac{\partial T}{\partial r}\right)\right]$$

$$\frac{\partial p}{\partial x}=p\left[-\frac{1}{u}\frac{\partial u}{\partial x}+\frac{1}{T}\frac{\partial T}{\partial x}-\frac{v}{pu}\frac{\partial p}{\partial r}-\frac{1}{u}\left(\frac{\partial v}{\partial r}+\frac{v}{r}\right)+\frac{v}{uT}\frac{\partial T}{\partial r}\right]$$

$$\frac{\partial k}{\partial x}=\frac{1}{\rho u}\left[-\rho v\frac{\partial k}{\partial r}-\rho\left(\tau_{rr}\frac{\partial v}{\partial r}+\tau_{rx}\frac{\partial u}{\partial r}+\frac{v\tau_{\phi\phi}}{r}\right)\right.$$
$$\left.-\rho\varepsilon+\frac{1}{\sigma_k}\frac{1}{r}\frac{\partial}{\partial r}\left(\rho\nu_t\frac{\partial k}{\partial r}r\right)\right]$$

$$\frac{\partial\varepsilon_s}{\partial x}=-\frac{v}{u}\frac{\partial\varepsilon_s}{\partial r}-c_{\varepsilon 1}\frac{\varepsilon_s}{k}\frac{1}{u}\left(\tau_{rr}^s\frac{\partial v}{\partial r}+\tau_{rx}^s\frac{\partial u}{\partial r}+\frac{v\tau_{\phi\phi}^s}{r}\right)$$
$$-(c_{\varepsilon 2}-\chi c_{\varepsilon 3})\frac{\varepsilon_s^2}{k}+\frac{1}{\rho u\sigma_\varepsilon}\frac{1}{r}\frac{\partial}{\partial r}\left(\rho\nu_t^s\frac{\partial\varepsilon_s}{\partial r}r\right)$$

$$\rho=\gamma M_j^2\frac{p}{T}$$

where

$$\chi=-\frac{k^3}{4\varepsilon_s^3}\left(\frac{\partial v}{\partial x}-\frac{\partial u}{\partial r}\right)^2\left(\frac{\partial v}{\partial r}+\frac{v}{r}\right)$$

$$\tau_{rr}=\frac{2}{3}k-\frac{2}{3}\nu_t\left(2\frac{\partial v}{\partial r}-\frac{v}{r}\right),\qquad\tau_{\phi\phi}=\frac{2}{3}k-\frac{2}{3}\nu_t\left(2\frac{v}{r}-\frac{\partial v}{\partial r}\right)$$

$$\tau_{xx}=\frac{2}{3}k+\frac{2}{3}\nu_t\left(\frac{\partial v}{\partial r}+\frac{v}{r}\right),\qquad\tau_{rx}=-\nu_t\frac{\partial u}{\partial r}$$

Appendix B: Mesh Design for the Marching Scheme

To make the marching scheme efficient, a multisize mesh design is adopted. The mesh distribution at the nozzle exit plane is as shown in Fig. A1. The innermost block consists of N mesh spacings of size Δr, where $N=N_0+N_1$. The next block consists of N_2 mesh spacings of size $2\Delta r$. The next block consists of N_4 mesh spacings of size $4\Delta r$, and so on. The mesh size increases by a factor of two when moving outward into the next block. In marching downstream, as soon as a location is reached, where the mixing-layer thickness is twice that of the initial thickness, every other mesh line in the innermost block is eliminated, and the block merges with the immediate adjacent block to form a single block with same size mesh. That is, from this location on, the innermost block has a mesh spacing (in the r direction) of $2\Delta r$. At this location the immediate adjacent block has a mesh spacing twice as large, namely, $4\Delta r$. The marching step Δx is now adjusted to a large value consistent with numerical stability requirement for a mesh size of $2\Delta r$ in the r direction. The marching resumes until a new location is reached, where the mixing-layer thickness doubles again. At this point, the process of eliminating every other mesh line to double the mesh spacing in the innermost block is repeated. The entire process repeats many times until the desired downstream location of the jet is reached.

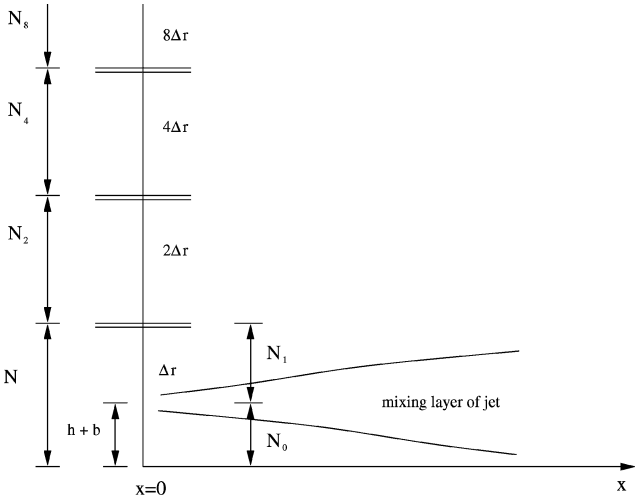

Fig. A1 Mesh distribution for the parabolized computer code.

In the present investigation, a 15-point stencil of the dispersion-relation-preserving scheme[15] is used to approximate the r derivatives in the innermost block of mesh. A 7-point stencil is used in all of the outer blocks. The reason for using a 15-point stencil is that the discretized equations in cylindrical coordinates are numerically weakly stable. To eliminate any grid-to-grid oscillations that are generated by the strong gradients in the jet mixing layer, 15-point artificial selective damping terms[20,21] are added to the computation algorithm. A 15-point damping stencil exerts essentially no damping on the mean flow solution (consisting of long waves). The number of mesh points N_1, N_2, N_4, etc., is chosen so that the grid-to-grid oscillations are nearly damped out before they can propagate out to reach the first mesh-size-change interface closest to the jet axis, where amplification may occur on reflection by the interface. In our code, the following parameters are used. $\Delta r=b/6$, where b is the half-width of the initial shear layer; $R_\Delta^{-1}=8.0$, where R_Δ is the mesh Reynolds number; $N_0=$ integer $[(h+b)/\Delta r]$, where h is the initial thickness of the potential core of the jet; $N_1=150(151)$ if N_0 is even (odd); and $N_2=76(75)$ if $\frac{1}{2}(N_0+N_1)$ is even (odd), etc. This mesh design is used in all of the computations in this work.

Acknowledgment

This work was support by the Aeroacoustics Research Consortium funded by a subcontract through the Ohio Aerospace Institute.

References

[1]Hanjalic, K., and Launder, B. E., "A Reynolds Stress Model for Turbulence and Its Application to Thin Shear Flows," *Journal of Fluid Mechanics*, Vol. 52, April 1972, pp. 609–638.

[2]Launder, B. E., and Spalding, D. B., "The Numerical Computation of Turbulent Flows," *Computer Methods in Applied Mechanics and Engineering*, Vol. 3, 1974, pp. 269–289.

[3]Launder, B. E., Reece, G. J., and Rodi, W., "Progress in the Development of a Reynolds Stress Turbulence Closure," *Journal of Fluid Mechanics*, Vol. 68, April 1975, pp. 537–566.

[4]Hanjalic, K., and Launder, B. E., "Contribution Toward a Reynolds Stress Closure for Low Reynolds Number Turbulence," *Journal of Fluid Mechanics*, Vol. 74, April 1976, pp. 593–610.

[5]Pope, S. B., "An Explanation of the Turbulent Round Jet/Plane Jet Anomaly," *AIAA Journal*, Vol. 16, No. 3, 1978, pp. 279–281.

[6]Sarkar, S., and Lakshmanan, B., "Application of a Reynolds Stress Turbulence Model to the Compressible Shear Layer," *AIAA Journal*, Vol. 29, No. 5, 1991, pp. 743–749.

[7]Thies, A. T., and Tam, C. K. W., "Computation of Turbulent Axisymmetric and Nonaxisymmetric Jet Flows Using the k–ε Model," *AIAA Journal*, Vol. 34, No. 2, 1996, pp. 309–316.

[8]Tam, C. K. W., Pastouchenko, N., and Auriault, L., "Effect of Forward Flight on Jet Mixing Noise from Fine-Scale Turbulence," *AIAA Journal*, Vol. 39, No. 7, 2001, pp. 1261–1269.

[9]Tam, C. K. W., and Auriault, L., "Jet Mixing Noise from Fine-Scale Turbulence," *AIAA Journal*, Vol. 37, No. 2, 1999, pp. 145–153.

[10]Brown, G. L., and Roshko, A., "On Density Effects and Large Structure in Turbulent Mixing Layers," *Journal of Fluid Mechanics*, Vol. 64, Pt. 4, 1974, pp. 775–816.

[11]Dimotakis, P. E., "Two Dimensional Shear Layer Entrainment," *AIAA Journal*, Vol. 24, No. 11, 1986, pp. 1791–1796.

[12]Tam, C. K. W., and Ganesan, A., "A Modified k–ε Turbulence Model for Calculating the Mean Flow and Noise of Hot Jets," AIAA Paper 2003-1064, Jan. 2003.

[13]Massey, S. J., Thomas, R. H., Abdol-Hamid, K. S., and Elimiligui, A. A., "Computational and Experimental Flow Field Analyses of Separate Flow Chevron Nozzles and Pylon Interaction," AIAA Paper 2003-3212, May 2003.

[14]Birch, S., Lyubimov, D., Secundor, A., and Yakubovsky, K., "Numerical Modeling Requirements for Coaxial and Chevron Nozzle Flows," AIAA Paper 2003-3287, May 2003.

[15]Tam, C. K. W., and Webb, J. C., "Dispersion-Relation-Preserving Finite Difference Schemes for Computational Acoustics," *Journal of Computational Physics*, Vol. 107, Aug. 1993, pp. 262–281.

[16]Lepicovsky, J., Ahuja, K. K., Brown, W. H., Salikuddin, M., and Morris, P. J., "Acoustically Excited Heated Jets, Part III—Mean Flow Data," NASA CR 4129, June 1988.

[17]Landau, L. D., and Lifschitz, E. M., *Fluid Mechanics*, Pergamon, London, 1959, Chap. 3.

[18]Seiner, J. M., Ponton, M. K., Jansen, B. J., and Lagen, N. T., "The Effects of Temperature on Supersonic Jet Noise Emission," AIAA Paper 92-02-046, May 1992.

[19]Tam, C. K. W., and Pastouchenko, N., "Noise from Fine-Scale Turbulence of Nonaxisymmetric Jets," *AIAA Journal*, Vol. 40, No. 2, 2002, pp. 456–464.

[20]Tam, C. K. W., Webb, J. C., and Dong, Z., "A Study of the Short Wave Components in Computational Acoustics," *Journal of Computational Acoustics*, Vol. 1, March 1993, pp. 1–30.

[21]Tam, C. K. W., "Computational Aeroacoustics: Issues and Methods," *AIAA Journal*, Vol. 33, No. 10, 1995, pp. 1788–1796.

W. J. Devenport
Associate Editor